High energy electron fluxes in dc-augmented capacitively coupled plasmas. II. Effects on twisting in high aspect ratio etching of dielectrics

Mingmei Wang[1,a)] and Mark J. Kushner[2,b)]
[1]*Department of Chemical and Biological Engineering, Iowa State University, Ames, Iowa 50010, USA*
[2]*Department of Electrical Engineering and Computer Science, University of Michigan, 1301 Beal Ave., Ann Arbor, Michigan 48109, USA*

(Received 14 September 2009; accepted 7 December 2009; published online 29 January 2010)

In high aspect ratio (HAR) plasma etching of holes and trenches in dielectrics, sporadic twisting is often observed. Twisting is the randomly occurring divergence of a hole or trench from the vertical. Many causes have been proposed for twisting, one of which is stochastic charging. As feature sizes shrink, the fluxes of plasma particles, and ions in particular, into the feature become statistical. Randomly deposited charge by ions on the inside of a feature may be sufficient to produce lateral electric fields which divert incoming ions and initiate nonvertical etching or twisting. This is particularly problematic when etching with fluorocarbon gas mixtures where deposition of polymer in the feature may trap charge. dc-augmented capacitively coupled plasmas (dc-CCPs) have been investigated as a remedy for twisting. In these devices, high energy electron (HEE) beams having narrow angular spreads can be generated. HEEs incident onto the wafer which penetrate into HAR features can neutralize the positive charge and so reduce the incidence of twisting. In this paper, we report on results from a computational investigation of plasma etching of SiO_2 in a dc-CCP using $Ar/C_4F_8/O_2$ gas mixtures. We found that HEE beams incident onto the wafer are capable of penetrating into features and partially neutralizing positive charge buildup due to sporadic ion charging, thereby reducing the incidence of twisting. Increasing the rf bias power increases the HEE beam energy and flux with some indication of improvement of twisting, but there are also changes in the ion energy and fluxes, so this is not an unambiguous improvement. Increasing the dc bias voltage while keeping the rf bias voltage constant increases the maximum energy of the HEE and its flux while the ion characteristics remain nearly constant. For these conditions, the occurrence of twisting decreases with increasing HEE energy and flux. © *2010 American Institute of Physics*. [doi:10.1063/1.3290873]

I. INTRODUCTION

Plasma etching of high aspect ratio (HAR) features for microelectronics fabrication is challenging state-of-the-art practices to obtain reproducible features with straight walls and definable shapes. For example, holes with diameters of tens of nanometers with aspect ratios (ARs) in excess of 70 are being fabricated for memory cells in large arrays. One of the challenging aspects of these processes is preventing the errant and nearly random occurrence of features that twist.[1] That is, instead of a feature etching vertically, the feature will twist or turn to the side. This often occurs after a significant fraction of the feature has already been etched. The direction of twisting, its frequency of occurrence and its proximity to other twisted features typically occurs randomly with no discernable pattern (see Fig. 1). The feature-to-feature etch rate can also significantly vary. Bowing is another anomalous behavior in which the sides of the feature bow out late during the etch.[2,3] Bowing, however, is typically a more reproducible and systematic effect. As shown in Fig. 1, the feature-to-feature bowing has less variation than the twisting and etch rate. Bowing is attributed to the change in the accep-

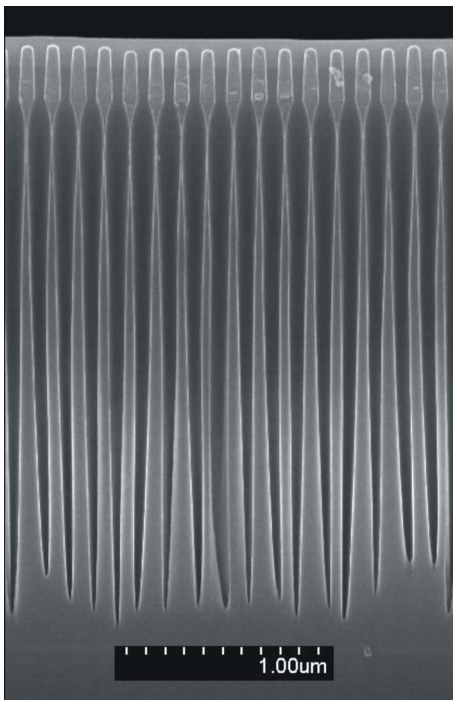

FIG. 1. (Color online) Scanning electron micrograph of an HAR array of SiO_2 features etched in a commercially available capacitively coupled plasma chamber using a fluorocarbon gas mixture. There is errant twisting and varied etching rate among trenches yet nearly uniform bowing.

[a)]Electronic mail: mmwang@iastate.edu.
[b)]Author to whom correspondence should be addressed. Electronic mail: mjkush@umich.edu.

tance angle of ions into the feature from the plasma due to erosion of the photoresist (PR) mask and subsequent reflection of ions from the facets of the PR.

Many explanations have been proposed for twisting, the majority of which attribute twisting to nonuniform macroscale parameters, such as ion and neutral energy-angular distributions and fluxes. These could, in principle, be controlled by adjusting reactor parameters (e.g., pressure,[4] bias power,[5] and frequency[6]). For example, methods have been proposed in the patent literature to control twisting by judicious choice of frequencies and powers in multifrequency excited capacitively coupled plasmas.[7] Optimizing these quantities have been demonstrated to reduce the incidence of twisting. Twisting can, however, occur errantly and randomly within a field of features having a pitch of only a few microns (see Fig. 1) whereas the scaling length for significant changes in the magnitude of fluxes and energy distributions of ions and neutrals is at least many millimeters in low pressure (<tens of mTorr) plasmas. Therefore, it is likely that sporadic twisting with feature-to-feature variations having many micron scale lengths may have causes in addition to variations in these macroscopic quantities (e.g., radial uniformity of fluxes) having scale lengths of many millimeters to centimeters.

A contributing explanation for feature-to-feature variations in profiles and twisting may originate from the small size of the feature open to the plasma. For example, for a hole 50 nm in diameter, the area of the opening to the plasma is 2000 nm^2. With this small opening, the rate of entry of radicals and ions into the feature begins to become statistical. The time between the arrival of two ions into a feature 50 nm in diameter for a flux of 10^{16} cm^{-2} s^{-1} is 5 μs. This small rate of particle arrival can lead to feature-to-feature statistical variations in both the identity and number of particles entering the feature. These statistical variations are particularly important in polymerizing gas mixtures for which the rate of etching depends not only on the ion energy but also the previous history of arrival of radicals which determines the polymer thickness and composition. Variations in fluxes that result in thicker polymer on one side of the feature compared to the other which slows its etch rate could produce asymmetric etch profiles.

The statistical variation of charged species into the feature (both ions and electrons) could also play in an important role in twisting. Charging of the surfaces inside the feature will occur in dielectric etching or in conductor etching using polymerizing gas mixtures which deposit an insulating layer that charges or traps charge. The statistical variation in charged particle fluxes into the feature could charge one side of the feature more than the other. This charging could then produce asymmetrical electric fields that deflect subsequent ions from the vertical and so produces twisting.

The charging of HAR features in plasma etching has been investigated by many researchers.[8–10] The general view of this process is that isotropic fluxes of low energy electrons negatively charge the top of the features. High energy positive ions which have a narrow angular distribution after being accelerated through the sheath penetrate deeper into features and positively charge the bottom of the feature. Depending on the thickness of the mask, which is typically charged negatively by thermal electrons, twisting, bowing, or microtrenching may occur.[11,12] In HAR etching, ions are usually energetic enough not to be significantly affected by the negative charge at the top of the feature and respond dominantly to the positive charge deeper in the feature. This process is dynamic. If the only effect was ions charging the bottom of the trench, the electric potential at the bottom of the trench would increase positively to the point of preventing further ion bombardment. At that point, only energetic neutrals originating from ions neutralized by grazing collisions with the side walls at the top of the feature would reach the bottom of the feature with sufficient energy to activate the etch. An alternate scenario is that electrons are attracted deep into the feature by the positive potential and neutralize positive charge which reduces the positive potential. This then allows further positive ion bombardment.

Many technologies have been developed to control or prevent intrafeature charging, one method being neutral beam etching.[13] One neutral beam technique is to extract ions from a plasma while neutralizing the ions by passing them through a grid.[14,15] Although very promising, this technique typically produces ions having lower incident energies with broader angular spreads than produced by high voltage rf biases. These fluxes may not be optimum for HAR application. A second method of controlling charging of features involves depositing a fluorocarbon or carbon film into the features which becomes mildly conductive after bombardment by high energy ions. The conductive film dissipates charge more quickly than the underlying SiO_2.[16] This technique has been specifically applied to the control of twisting by reducing intrafeature charging.[17] A third method is injecting negative charge into the feature to neutralize accumulated positive charge. There are two approaches to reach this goal. One approach utilizes pulsed ion-ion plasmas to inject negative ions into the feature.[18,19] The second approach, investigated here, produces and injects a narrow angle, high energy electron (HEE) flux into the feature.

HEE fluxes onto wafers can be produced in dc-augmented capacitively coupled plasmas (dc-CCPs). In these reactors, a dc voltage is applied to the electrode opposite the rf biased substrate. Secondary electron emission from the dc biased substrate produces HEE fluxes having energies up to a few keV with angular spreads of $<0.5°$. The characteristics of HEE fluxes produced in dc-CCP reactors were discussed in Part I,[20] including a review of prior works.[21–23]

In this paper, results are discussed from a computational study of a dc-CCP for etching of HAR features in SiO_2 over Si. The model system is a parallel plate CCP with a 10 MHz bias on the lower electrode; and a dc bias on the upper electrode. Characteristics of dc-CPP's sustained in $Ar/C_4F_8/O_2$ and properties of HAR etch profiles with and without HEE fluxes are discussed. We found that the occurrence of twisting generally decreases with increasing HEE fluxes and increasing maximum energy of that flux. This effect is attributed to the penetration of electrons into the features which neutralize positive charge.

The models used in this investigation are described in Sec. II followed by our discussion of properties of dc-CCPs

sustained in $Ar/C_4F_8/O_2$ mixtures in Sec. III and HAR etched features in Sec. IV. Our concluding remarks are in Sec. V.

II. DESCRIPTION OF THE MODELS

The two-dimensional (2D) Hybrid Plasma Equipment Model (HPEM) was used for reactor scale simulation. The HPEM has been previously discussed in detail in Ref. 24 and in Part I,[20] and so is only briefly described here. The HPEM is a 2D model which consists of separate modules which address different physical phenomena. Each module consists of a time integration over many rf cycles, during which quantities (e.g., densities and temperatures) are either recorded as a function of position and phase or recorded only as position dependent quantities averaged over the rf cycle. These values are then passed to the next module and the process iterated to a cycle-average steady state. The modules used in this study are: (1) the Electron Monte Carlo Simulation for sheath accelerated secondary electrons, (2) the Fluid Kinetics Module to obtain densities, fluxes and energies of all charged and neutral species, as well as the electric potential from the solution of Poisson's equation, and (3) the Plasma Chemistry Monte Carlo Module (PCMCM) to obtain the energy and angular distributions (EADs) of neutrals and charged species striking the wafer. These species include the high HEEs incident onto the wafer resulting from secondary electron emission from all surfaces and the dc electrode in particular. See Part I for a discussion of the techniques for computing the energy spectrum of the HEE flux.[20] The gas phase reaction mechanism used for the $Ar/C_4F_8/O_2$ gas mixture is the same as in Ref. 25.

The fluxes of reactant species and their EADs from the PCMCM are then used as input to the Monte Carlo Feature Profile Model (MCFPM).[26] The MCFPM resolves the surface (e.g., PR, polymer, and semiconductor) of the wafer using a 2D rectilinear mesh. Poisson's equation is solved to obtain charge induced potentials and electric fields in and around the feature. Charges from incident electrons and ions are accumulated and summed on the mesh. The charge may subsequently move as explained below. If a mesh cell with charge is removed by virtue of neutral chemical reactions, its charge is retained in the mesh by redistributing it to the adjacent mesh cells.

In the MCFPM, pseudoparticles representing ions and neutral species are launched toward the surface with a frequency, energy, and angle randomly chosen from the EADs produced by the PCMCM. Each particle carries a weighting of atoms/s or current. The number of atoms per pseudoparticle is equal to the number atoms in a solid mesh cell. Although this choice only affects resolution in the absence of charging, when including charging, the results are sensitive to the size of the cell (see discussion below.) Each gas phase particle is tracked until it is either incorporated into the solid mesh or leaves the computational domain. The trajectories of gas phase particles produced by the interaction of fluxes with the surface (e.g., an etch product) are then also followed until that particle is incorporated into the solid mesh or leaves the domain. Since the residence time of a particle in a feature is at best a nanosecond whereas the time between incident particles having the largest fluxes is many microseconds, the likelihood of finding two incident particles in the feature at the same time is small. As a result, only a single gas phase pseudoparticle is tracked at a time. If more than a single gas phase particle is produced as a result of a surface reaction, the trajectory of the first particle is completed before the trajectories of the second (and subsequent particles) are followed.

We assumed that all ions striking a surface deposit their charge at the site of the collision. The ion then reflects as a hot neutral, diffusively at low energy, and progressively more specularly as its energy increases. Electrons striking the surface either deposit their charge or are reflected based on the secondary emission coefficient for electrons by electrons γ_{ee}. Electrons striking a surface having values of $\gamma_{ee}<1$ on the average deposit negative charge. Electrons striking a surface with values of $\gamma_{ee}>1$ on the average produce positive charging. The energy and angular dependence of γ_{ee} we used were obtained from Ref. 27. Given the limited materials for which properties were available, we used γ_{ee} values for quartz to represent SiO_2, Si, and PR; and values of γ_{ee} for Teflon for fluorocarbon polymer. These algorithms were implemented in the following manner. When an electron strikes the surface, its energy and angle of incidence were used to obtain γ_{ee}. A random number r [distributed (0,1)] was selected. If $r>\gamma_{ee}$, the electron was collected on the surface. If $r<\gamma_{ee}$ the electron was reflected.

The EADs of ions and neutral particles, and of HEE fluxes, were obtained from the PCMCM of the HPEM, as discussed in Part I.[20] The fluxes of thermal electrons are not directly obtained from the PCMCM and so these fluxes are computed in the following manner. Since the wafer is capacitively coupled to ground, the net cycle-averaged charged particle flux to its surface must sum to zero. The fluxes obtained from the PCMCM for ions and HEEs are separately summed. The net current at this point is positive due to the absence of thermal electrons. The charge neutrality requirement is then achieved by adding a thermal electron flux having Maxwellian energy distribution and a Lambertian angular distribution. The electron temperature is obtained from the HPEM.

Given the charge accumulation on surfaces, Poisson's equation, $\nabla\cdot\varepsilon\nabla\Phi=-\rho$ is solved using the method of successive over-relaxation to provide the electric potential Φ in and around the feature for permittivity ε and charge density ρ. The conductivity σ and permittivity of solid materials are specified. Since it is computationally expensive to solve Poisson's equation, the electric fields are not necessarily updated after the trajectory of each charged particle is completed (which may produce charge on the surface of the feature). Instead, Poisson's equation is solved after launching a specified number of charged particles—typically 30 in the cases discussed here. We parameterized this number to ensure that computed values of Φ were well represented. The boundary conditions were $\Phi=0$ at the top and bottom boundaries of the computation domain, and $d\Phi/dx=0$ at the left and right boundaries.

We also included dispersal of the charge in the solid

materials due to conduction currents. The charge density for cell j used in solution of Poisson's equation was given by

$$\frac{d\rho_j}{dt} = \frac{d}{dt}\left(\sum_i \frac{q_i}{V_j}\right) - [\nabla \cdot \sigma(-\nabla\Phi)], \quad (1)$$

where q_i is the charge of incident particle i, V_j is the volume of cell j, and σ is the material conductivity. Since the likelihood that two gas phase charged particles will be in the feature at the same time is extremely small, we did not include charge in the gas phase in solution of Poisson's equation. Collected charge remains on surfaces until neutralized by subsequently collected particles or dispersed by conduction through the material. We did not allow that a sputtered material cell would carry away its charge into the gas phase. So when a cell with charge is sputtered, its charge is dispersed to adjoining solid cells. We do, however, allow charge to be buried. That is, if a cell is charged and deposited over by polymer, the charge remains below the surface.

The reaction mechanism for etching of Si and SiO_2 in fluorocarbon plasmas is described in detail in Ref. 26. Briefly, etching of SiO_2 is dominantly through formation of a fluorocarbon complex. SiO_2 sites on the surface are first activated by ion bombardment

$$SiO_2(s) + M^+(g) \rightarrow SiO_2^*(s) + M^*(g), \quad (2)$$

where SiO_2^* represents an activated site on surface, M^+ is an ion and M^* is its hot neutral counterpart. Then C_xF_y neutrals react with the activated SiO_2 sites to produce a complex layer

$$SiO_2^*(s) + C_xF_y(g) \rightarrow SiO_2C_xF_y(s). \quad (3)$$

Further deposition by C_xF_y neutrals produces a thicker polymer layer $(C_xF_y)_n$. Energetic ions and hot neutrals penetrate this polymer layer and reach the complex to sputter it, with carbon from the polymer layer providing a means to remove the oxygen in the oxide,

$$SiO_2C_xF_y(s) + M^+(g) \rightarrow SiF_y(s) + CO_2(g) + M^*(g). \quad (4)$$

The remaining Si is etching dominantly by F atoms diffusing through the polymer layer, passivating the Si followed by ion activation

$$SiF_{n-1}(s) + F(g) \rightarrow SiF_n(s), \quad n < 4, \quad (5)$$

$$SiF_n(s) + M^+(g) \rightarrow SiF_n(g) + M^*(g), \quad (6)$$

$$SiF_3(s) + F(g) \rightarrow SiF_4(g). \quad (7)$$

Oxygen radicals produced by electron impact of O_2 are used to control the thickness of the polymer layer during etching

$$(C_xF_y)_n(s) + O(g) \rightarrow (C_xF_y)_{n-1}(s) + COF_x(g). \quad (8)$$

Sputtering and redeposition of the PR mask were also included using a similar mechanism as polymer removal though at a lower rate. The reaction probabilities for the PR were chosen to provide an etch selectivity of about 10-to-1 with respect to SiO_2. (That is, the each rate of the PR is 0.1 that of SiO_2.)

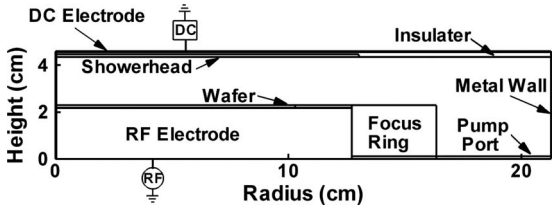

FIG. 2. Schematic of a dc-augmented, cylindrically symmetric single frequency CCP reactor.

Experimentally, twisting can be rare, occurring in only a few percent or less of all features. Computationally, this presents challenges as many hundreds to thousands of features would need to be simulated in order for a statistically significant number of twisted features to be obtained. The required resolution of the mesh also presents challenges. It is common that the numerical mesh in Monte Carlo simulations be larger than atomic dimensions, typically a few nanometers. A mesh cell could then represent hundreds of atoms, which would also apply to the gas phase pseudoparticles. When including charging, we found that there was a mesh size dependence to the calculation which was only resolved by having the mesh size (and gas phase pseudoparticles) represent single atoms. This unfortunately, resulted in total simulation times for hundreds of cases for each process condition which were unacceptably large. After extensive parameterizations on this dependency, we chose a mesh size of 5 nm and reduced the charge per particle so that computer times were acceptable and the results were essentially the same as when using meshes with atomic dimensions. We also chose values that accentuated the propensity of twisting so that acceptable statistics could be obtained with only tens of cases per process conditions as opposed to hundreds to thousands of cases. We again confirmed that other than increasing the frequency of twisting, other etch properties were well represented compared to using smaller cells and charge.

III. BULK PLASMA PROPERTIES

A schematic of the cylindrically symmetric dc-CCP reactor used in this study is shown in Fig. 2. The chamber is 43 cm in diameter. The powered substrate is 26 cm in diameter, and holds a 20 cm diameter Si wafer which is surrounded by a 3 cm wide Si disk. A focus ring $(\varepsilon/\varepsilon_0=8)$ extends beyond the Si disk to a diameter of 32 cm. The substrate is powered at 10 MHz through a blocking capacitor. The rf voltage was adjusted to deliver a specified power unless noted otherwise. The metal showerhead, having a diameter of 26 cm, is embedded in a dielectric $(\varepsilon/\varepsilon_0=8)$ and is dc biased. The dc voltage was also adjusted to deliver a specified power. The wafer to showerhead gap is 2 cm. The annular pump port extends from the focus ring to the outer metal wall. The secondary emission coefficient by ion bombardment on all surfaces is $\gamma=0.15$. The notation used to describe these voltages are: V_{rf} is rf voltage applied to the substrate, V_{rf0} is the self dc bias on the rf electrode, and V_{dc} is the dc bias applied to the upper electrode.

The base case operating conditions are $Ar/C_4F_8/O_2 = 80/15/5$ at 40 mTorr with a flow rate of 300 sccm (where

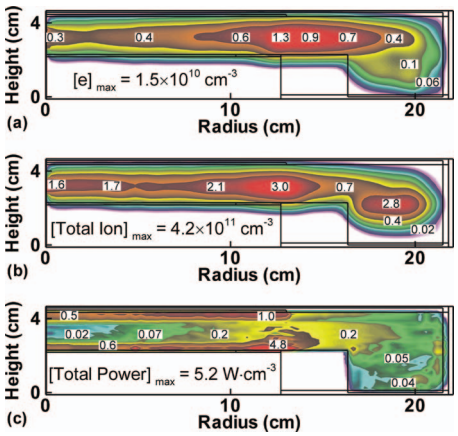

FIG. 3. (Color) Bulk plasma properties for the base case ($Ar/C_4F_8/O_2$ =80/15/5, 40 mTorr, 300 sccm, P_{rf}=1 kW at 10 MHz, P_{dc}=200 W). (a) Electron density, (b) total ion density, and (c) power deposition. The maximum value in each frame is noted.

sccm denotes standard cubic centimeter per minute at STP.) The substrate is powered at 1 kW (V_{rf}=650 V, V_{rf0}= −115 V) and the dc electrode delivers 200 W (V_{dc}= −370 V). The rf cycle-averaged electron density, total positive ion density, and power deposition density are shown in Fig. 3 Both the electron density and total ion density have edge-peaked distributions, partly a result of the low frequency being largely electrostatically coupled with electric field enhancement at the edge of the Si ring. The low AR of the reactor could also lead to this edged peak in ion density. The electron density has a maximum value of 1.5×10^{10} cm^{-3} and the positive ion density has a maximum value of 4.2×10^{11} cm^{-3} producing an electronegativity of about 30. The power deposition along the surface of both electrodes is also edge peaked with a maximum value of 5.2 W cm^{-3}. In this narrow gap CCP the sheaths occupy near 20% of the gap width, a condition exacerbated by the additional sheath thickness attributable to the dc bias.

The EADs of all ions and HEEs incident onto the wafer are shown in Fig. 4. Note that the energy distributions for HEEs are only for those electrons that originate from secondary emission from any surface, as described in Part I.[20] The plasma potential at different times during the rf cycle is shown in Fig. 5. As discussed in Part I, ion fluxes incident onto the dc and rf electrodes produce secondary electrons which are accelerated, nearly collisionlessly, into the plasma by the dc and rf sheaths. The majority of HEE incident onto the wafer originate by secondary emission from the dc electrode.[20] Since the time to cross the gap for the HEEs from the dc electrode is short compared to the rf period, the range of the energies of the HEEs reflects the instantaneous difference between the sheath potential on the dc and rf sides of the reactor during the rf cycle. As shown in Fig. 5, electrons emitted at the peak of the anodic part rf cycle gain the full dc and rf potentials (diminished by the dc bias on the substrate) as the plasma potential is raised to its theoretical maximum value, $\varepsilon_{max}=-V_{dc}+V_{rf}+V_{rf0}$=905 eV. The calculated HEE flux has a maximum energy of ε_{max}=882 eV. Secondary electrons emitted from the dc electrode during the cathodic part of the rf cycle could be trapped in the plasma.

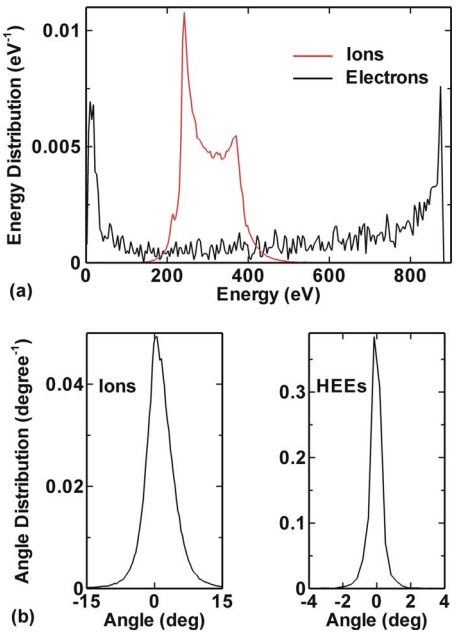

FIG. 4. (Color online) EADs summed for all ions and HEEs incident onto the wafer for the base case ($Ar/C_4F_8/O_2$=80/15/5, 40 mTorr, 300 SCCM, P_{rf}=1 kW at 10 MHz, P_{dc}=200 W). (a) Energy distributions and (b) angular distributions. In general the HEE have a narrower angular spread than the ions.

These electrons do not gain enough energy in the dc sheath to climb the negative potential of the rf sheath. About 30% of the HEEs striking the wafer originate from secondary emission from the wafer, though these electrons tend to be at energies <100–150 eV, as discussed in Part I.

With 1 kW of bias power, the majority of ions are incident on the wafer with energies of 200 to 450 eV, with an angular spread of ±8° as shown in Fig. 4(b). In comparison, the HEE flux has an angular spread of ±0.5° [also shown in Fig. 4(b)]. The total positive ion flux (at r=5 cm) is 5×10^{15} cm^{-2} s^{-1} and the HEE flux is 1×10^{15} cm^{-2} s^{-1}, yielding a thermal electron flux of 4×10^{15} cm^{-2} s^{-1}.

IV. EFFECT OF CHARGING AND HEE FLUXES ON PROFILES OF HAR FEATURES

To investigate the effects of charging on twisting of SiO_2 features, 41 identical trenches were simulated with different

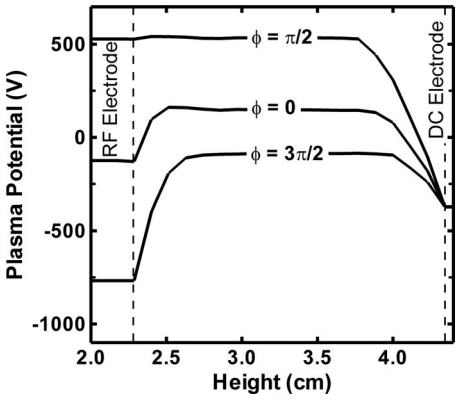

FIG. 5. Plasma potential as a function of chamber height and phase for the base case. The energy of the HEE flux originating from the dc electrode at any time during the rf cycle is nearly the difference between the dc and rf biases.

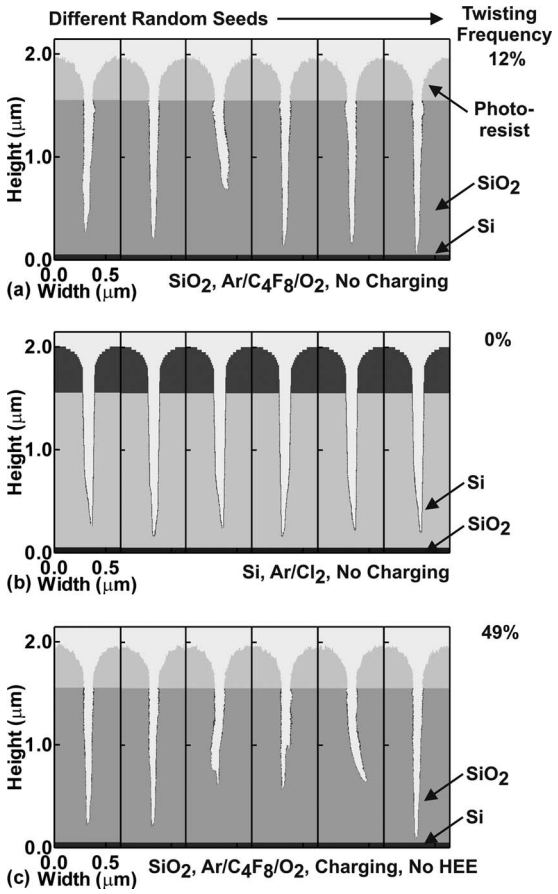

FIG. 6. Profiles selected from 41 otherwise identical simulations except for using different random number seeds. The reactor conditions are the base case except for the rf power being 4 kW. (a) Fluorocarbon plasma etching of SiO_2 without including charging. (b) Ar/Cl_2 plasma etching of Si without including charging. (c) Fluorocarbon plasma etching of SiO_2 including charging but no HEE fluxes. The twisting frequency for each case is noted. Twisting occurs in the absence of charging for polymerizing gas mixtures.

random seeds for each process starting condition. The use of different random number seeds in the calculation provides a different sequence of particles (i.e., identity, energy, and angle) randomly selected from the same EADs provided by the HPEM. This also produces a different sequence of randomly chosen reactions of gas phase particles with the surface. This procedure emulates a set of adjacent side-to-side features which randomly receive different fluxes. We confirmed this by simulating a number of cases having six side-by-side features in the same mesh. There were few, though discernable, feature-on-feature effects. (Computationally, it is faster to simulate six cases each having a single trench in the mesh than six trenches in a single mesh.) The mask opening is 75 nm wide with a depth of 1500 nm to a Si stop layer, yielding an AR of 20. The PR is initially dome-shaped with a maximum thickness of 450 nm. For incident ion energies <1.3 keV, polymer deposition effectively stops etching at the Si layer.

A selection of trenches for a substrate power of 4 kW is shown in Fig. 6. These profiles are a subset of all cases that were run. They were chosen to provide representative, and in some cases extreme, samples of features and do not necessarily represent the average. Profiles are shown in Fig. 6(a) without considering charge deposition and so ignore the consequences of electric field deflections on ion trajectories. The majority of profiles are straight—only five trenches of 41 displayed twisting or about 12%. Note that the straight features have different etch rates. Even for a uniform flux of reactants on the wafer scale, due to the small opening to the feature, there are statistical variations in the order, identity, and energy of particles entering adjacent trenches. For ion fluxes of 10^{16} cm^{-2} s^{-1}, the interval between ions entering a circular via is about 1 μs. The statistical nature of the incident fluxes is even more pronounced for ions in the high energy tail of the ion energy and angular distribution (IEAD) which already has a small population. These are the ions which are most responsible for activating etch processes. The end result is a feature-to-feature difference in etch rate.

The cause for the occasional twisting and the variation in etch rate for this process may have two components—the statistical variation in the sequence of particles entering the feature and the statistical variation in ion energies. The more rapid buildup of polymer or more etching on one side of the trench due to statistical variation in fluxes and reaction rates can slow the etch rate on that side of the trench and produce an asymmetric profile. Since few ions reach the bottom of the trench without neutralizing grazing collisions off the sidewalls, once a feature begins to twist, it tends to be self-perpetuating. The randomness of the polymer deposition can also contribute to variations in etch rates.

To provide insights to how much of the twisting and variation etch rates is due to randomness in polymer deposition and how much is due to randomness in ion energies, the etching of Si trenches in Ar/Cl_2 gas mixtures was simulated. The same initial profile and AR as those of the SiO_2 features were used and, again, charging was not considered. The mechanism for etching of Si using Ar/Cl_2 plasmas is by passivation of Si by Cl atoms forming $SiCl_x$ $(x \leq 3)$ surface species, followed by ion activated etching to evolve gas phase $SiCl_x$.[28,29] There is typically no significant polymer deposition. These processes have been included in a reaction mechanism in our feature profile model, as discussed in Ref. 30.

Examples of Si profiles etched in Ar/Cl_2 plasmas are shown in Fig. 6(b). The flux of Cl atoms (1.4×10^{18} cm^{-2} s^{-1}) greatly exceeds that of ions (3.5×10^{16} cm^{-2} s^{-1}) and so statistical variations in fluxes (and their energies and angles) can be attributed dominantly to the ions. No significant twisting is predicted but there are feature-to-feature variations in etch rates. We attribute these differences to the statistical variation in the flux and energy of ions incident into adjacent features. We can therefore conclude that even in the absence of charging, the statistical nature of incident species in highly polymerizing processes can produce some small amount of twisting. Feature-to-feature variations in etch rates, even for nonpolymerizing chemistries, can occur due to the randomness in the magnitudes, energies and angles of the ion fluxes.

When including charging in the SiO_2 etch process, the incidence and severity of twisting are both increased, as shown in Fig. 6(c). In these cases, the HEE flux was not included and so the only electron flux incident onto the fea-

tures is that from the thermal electrons having a temperature of about 2 eV. The incidence of twisting increased from 5/41 (or 12%) without charging to 20/41 (or about 49%) with charging. The increase in twisting largely results from there being immobile charge deposited on the sidewalls which creates lateral electric fields which deflect the ions. (See discussion below.) The effect is exacerbated by the trapping of charge in the polymer layers where charge is deposited over. Given a nonconducting polymer (as is the case here) there is no way to dissipate the charge in the absence of sputtering away the overlying polymer. Since the removal rate of polymer on the side wall is slow as ion trajectories are grazing (with low sputtering rates), the trapped charge persists. In a sense, the trapped charges act as sentinels which produce persistent electric fields which perpetuate the twisting.

If the polymer has a finite conductivity, it may be possible to dissipate some of the accumulated charge and so lessen the likelihood of twisting.[16] We investigated this possibility by specifying the conductivity of the polymer to be 0.01 Ω^{-1} cm^{-1}. The incidence of twisting decreased from 49% to 38%, an improvement on but not an elimination of twisting. Since the underlying SiO_2 is not conductive, charge transmitted through the polymer can still accumulate at the SiO_2 interface. If the polymer is thin, it will not totally shield the charges and so electric fields capable of deflecting ions are still able to penetrate into the trench. The side wall is also not uniformly and continuously covered by polymer, and so some of the incident charge deposits directly on the SiO_2, which then creates deflecting electric fields.

In order for the conductivity of the bounding materials of the trench to have a significant effect on reducing or eliminating twisting, the bulk material should be conductive. For example, if the polymer is nonconductive while SiO_2 is artificially made highly conductive (0.01 Ω^{-1} cm^{-1}), the twisting frequency is reduced to 25%, about half that of the base case. Since the polymer layer is thin and not of uniform coverage, the charge that is directly deposited on the SiO_2 is conducted away. If both the polymer and SiO_2 are conductive, charging has only a small effect on incident ion trajectories. In this case, the frequency of twisting is comparable to that when ignoring charging effects, about 12%. These results are consistent with experimental reports of twisting in Si etched in fluorocarbon gas mixtures, particularly if the overlying polymer is thick. This corresponds to the case of a nonconducting polymer and a conducting substrate in our investigations.

In these simulations we used an initially dome-shaped PR profile. The shape and subsequent faceting of the PR by plasma erosion are known to affect the shapes of features, such as the bowing near the top of the feature shown in Fig. 1. We have not done detailed studies on the possible consequences of initial PR profiles (and their erosion) on twisting. However, since twisting is likely a result of statistical variations in fluxes and charging, neither of which is dominantly a function of the PR profile, we do not expect twisting to have a first order dependence on the PR profile. The thicker the PR in comparison to the feature depth, the greater the likelihood that charging of the PR might contribute to twisting by perturbing trajectories of incoming ions.

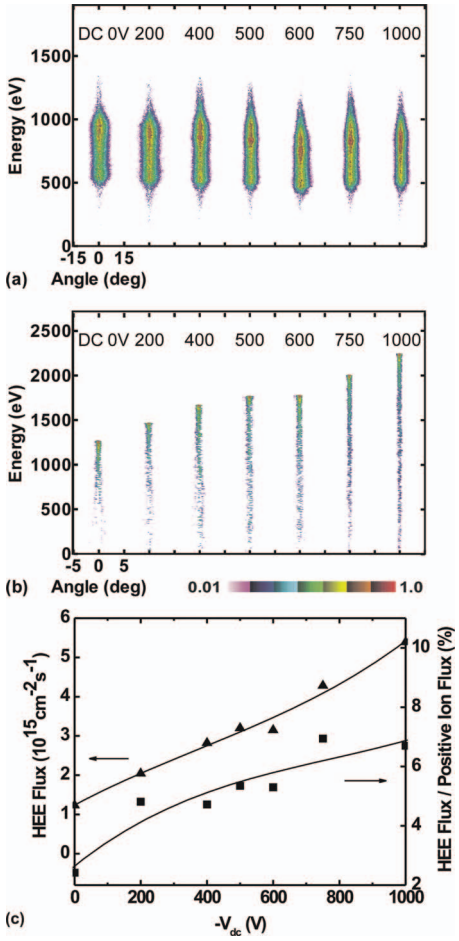

FIG. 7. (Color) HEE and ion characteristics as a function of V_{dc}. V_{rf} was held constant at 1500 V while V_{rf0} was allowed to seek its self consistent value. (a) IEADs, (b) EADs of the HEE fluxes, and (c) HEE flux and fraction of HEE flux with respect to the positive ion flux. Contour plots are 2 decades on a log-scale.

One of the intents of the dc-augmentation of a CCP reactor is to produce HEE fluxes with a narrow angular spread that are able to penetrate into features to neutralize positive charge. For example, EADs for all ions and HEE fluxes for dc voltages of $V_{dc}=0$ to -1000 V are shown in Fig. 7. Instead of adjusting the rf voltage to maintain a constant power, the rf voltage was kept constant to minimize the change in the IEADs and so minimize its influence on the evolution of feature profiles. We did, however, allow V_{rf0} to vary so that the charging of surfaces would be self-consistently accounted for. So in spite of holding V_{rf} constant, the IEADs vary slightly in energy as V_{dc} increases due to the variation in V_{rf0}, though these small changes are not particularly significant. The narrowing in angle of the IEADs with increasing (more negative) V_{dc} results from an increase in plasma density and narrowing of the sheath produced by the ionization from secondary electrons accelerated by the dc bias.

The range in energy of the HEE generally reflects the instantaneous difference between the sheath potential on the dc and rf sides of the reactor during the rf cycle. (Recall that these distributions are only for electrons and their progeny that result from secondary electron emission.) The maximum energies for electrons emitted from the dc electrode generally

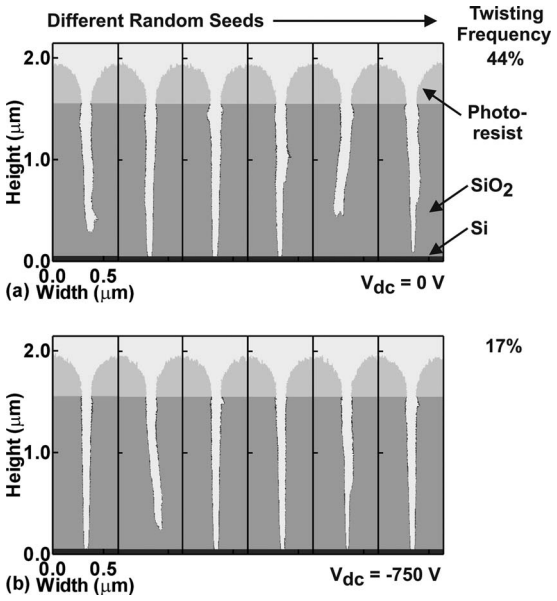

FIG. 8. Profiles of otherwise identical trenches for fluorocarbon plasma etching of SiO_2 over Si chosen from 41 trials with different random number seeds when including charging and HEE fluxes. (a) $V_{dc}=0$ and (b) $V_{dc}=-750$ V. The twisting frequency for each case is noted and decreases when increasing V_{dc} (more negative).

obey the scaling law $\varepsilon_{max}=-V_{dc}+V_{rf}+V_{rf0}$ with values of 1270 to 2200 eV for $V_{dc}=0$ to -1000 V. Note the HEE beams that are naturally produced due to the oscillation of the plasma potential even with $V_{dc}=0$ V. The additional use of dc augmentation is meant to control the extent of the energy and the magnitude of the flux of these secondary electrons.

The magnitude of the fluxes of HEEs and the fraction of the HEE flux compared to the ion flux are also shown in Fig. 7 as a function of V_{dc}. The magnitude of the HEE flux increases from 1.2×10^{15} to 5.5×10^{15} cm^{-2} s^{-1} for $V_{dc}=0$ to -1000 V. This represents 9.5% to 58% of the total ion flux. There is a commensurate decrease in the thermal electron flux which charges the top of the feature, and an increase in the dc current which flows to the side walls. [See Part I (Ref. 20) for a discussion of the disposition of dc current.]

Profiles obtained with HEE fluxes when including charging for $V_{dc}=0$ and -750 V are shown in Fig. 8. Different random number seeds were used for 41 cases each and representative profiles are shown. The occurrence of twisting for $V_{dc}=0$ is 18/41 or 44%, only marginally better than in the absence of HEE fluxes. For $V_{dc}=-750$ V, the occurrence of twisting is 7/41 or 17%, only slightly higher than in the absence of charging. The HEEs apparently successfully penetrate into the trench and neutralize sufficient positive charge to reduce the production of lateral electric fields by positive ions. In particular, positive charge is neutralized before it is trapped in the polymer by further deposition. The decrease in the incidence of twisting between $V_{dc}=0$ and -750 V is attributable to at least two factors—an increase in the electron energy which produces more forward scattering and an increase in the magnitude of the HEE flux [Fig. 7(c)]. Between $V_{dc}=0$ and -750 V, the electron flux increases from 9.5% to 39% as a fraction of the total ion flux.

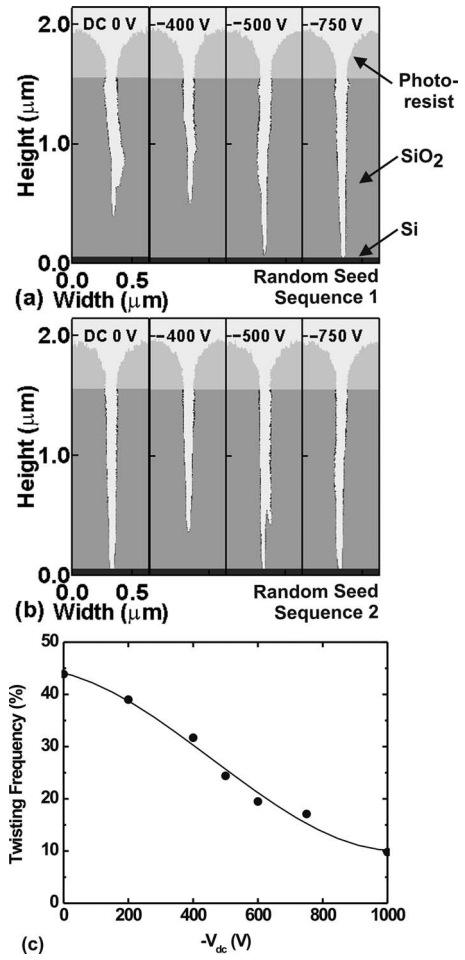

FIG. 9. Profiles and twisting frequency as a function of V_{dc}. (a) Profiles for different values of V_{dc} of otherwise identical trenches for fluorocarbon plasma etching of SiO_2 over Si chosen from 41 trials. (b) Same as in (a) except for different random number seeds. (c) Twisting frequency as a function of V_{dc}. The twisting frequency and etch rate generally decrease with increasing (more negative) V_{dc}.

Profiles obtained with HEE fluxes and charging for $V_{dc}=0$, -400, -500, and -750 V on are shown in Fig. 9 for constant etching times. These are representative features from 41 simulations with different random seeds. Although there is some variation in etch rate, more negative V_{dc} tends to increase the etch rate. In our reaction mechanism the HEE fluxes do not directly affect surface chemistry by initiating reactions. The higher etch rates likely result from a larger ion flux resulting from the ionization produced by the HEE. The ions in the feature also have higher energy due to the reduction in the positive potential in the trench by neutralization by the HEE flux. With a smaller intrafeature electric field, incident ions are in general less impeded in both vertical and lateral directions. The twisting frequency as a function of V_{dc}, shown in Fig. 9(c), decreases with increasing (more negative) V_{dc}, from 44% at $V_{dc}=0$ to 10% at $V_{dc}=-1000$ V.

Time sequences of electric potential distributions as etching proceeds are shown in Fig. 10 for otherwise identical cases with different random seeds. One random number seed produced a straight feature while the other random number seed produced twisting. The conditions are $P_{rf}=4$ kW and $V_{dc}=-750$ V. The maximum potential in the trench is 100–

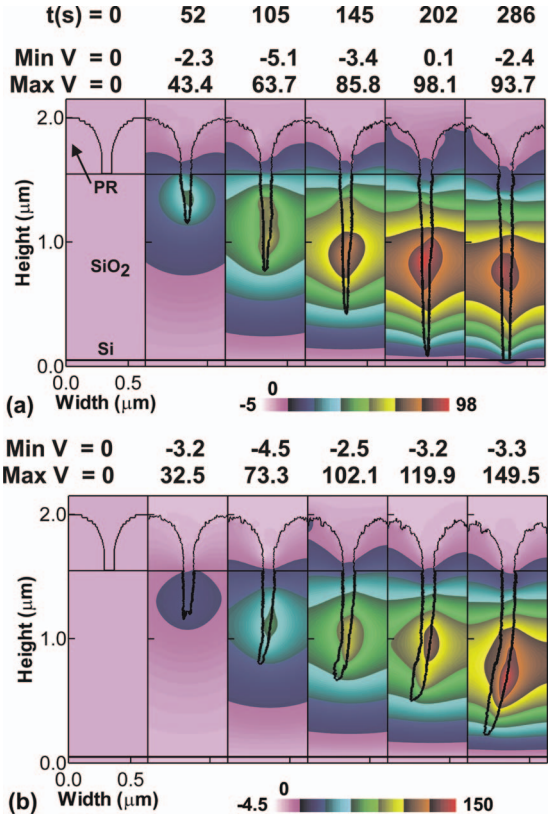

FIG. 10. (Color) Time sequence of potential distributions in features as etching proceeds differing only in the choice of random number seeds. (a) Straight trench and (b) twisted trench. The conditions are P_{rf}=4 kW and V_{dc}=−750 V. The time, and the minimum and maximum voltage for each profile are noted.

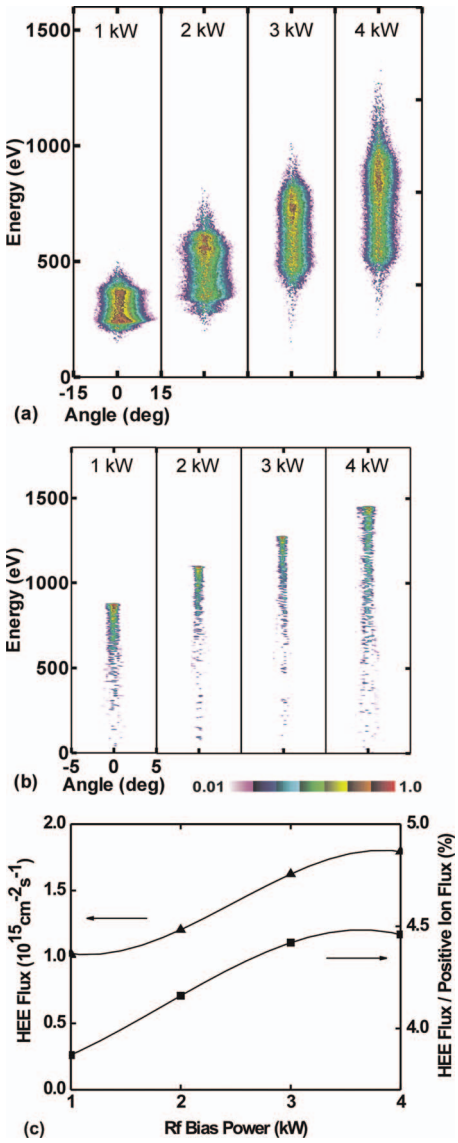

FIG. 11. (Color) Consequences of rf bias power while keeping the dc power constant. (a) IEADs for P_{rf}=1–4 kW, (b) EADs for the HEE flux and (c) HEE flux and fraction of HEE flux with respect to the positive ion flux as a function of P_{rf}. Contour plots are 2 decades on a log-scale.

150 V and occurs roughly half-way down the trench or at an AR=10. This is approximately the location that the average ion would strike the side wall and deposit charge. Features with smaller ARs where ions strike the bottom of the trench before reflecting off the side walls will have the maximum in potential on the bottom of the feature. The top of the mask charges to only a few volts negative. The maximum positive potential increases with increasing depth as the likelihood for electron penetration into the feature decreases.

When the statistical distribution of charged particles produces a potential that is basically symmetric across the trench, the lateral electric fields are small and there is little off-axis deflection of ions. The end result is a nearly straight feature, as shown in Fig. 10(a). If the statistical distribution of ions and electrons produces more positive charge and a larger potential on one side of the feature, as shown in Fig. 10(b), the lateral electric fields are more intense. These fields produce a deflection in the ion trajectory which contributes to twisting. The twisted feature has a larger positive potential, likely a result of positive charge being trapped in the polymer and so is shielded from directly being neutralized by the HEE flux.

Holding the dc bias power constant at 200 W, we investigated the effects of rf bias power on EADs and HEE fluxes. For example, the EADs for HEEs and ions, and HEE fluxes for rf powers of 1 to 4 kW are shown in Fig. 11. With increasing rf bias power, the extent in energy and flux increases for both ions and electrons. These increases in energy result from the increase in V_{rf} (650 V at 1 kW to 1450 V at 4 kW) and V_{rf0} (−120 V at 1 kW to −220 V at 4 kW). However since the dc current and HEE flux also increase with rf power, V_{dc} decreases (becomes less negative) to deliver a constant dc power (−370 V at 1 kW to −250 V at 4 kW). The end result is that the increase in ε_{max} (470 eV at 1 kW to 1200 eV at 4 kW) scales less than linearly with V_{rf}. The extent of the EADs is also less than linear with power. The HEE flux as fraction of the ion flux, shown in Fig. 11(c), does not significantly change as a function of V_{rf}.

The twisting frequency as a function of rf power is shown in Fig. 12 with and without HEE fluxes. The narrowing in angle of the ion flux with rf power increases the penetration of positive charge deeper into the feature prior to the ion fluxes being neutralized by colliding with the side walls. The increase in ion energy offsets the beneficial effects of the neutralizing HEE flux. Although there is a decrease in the

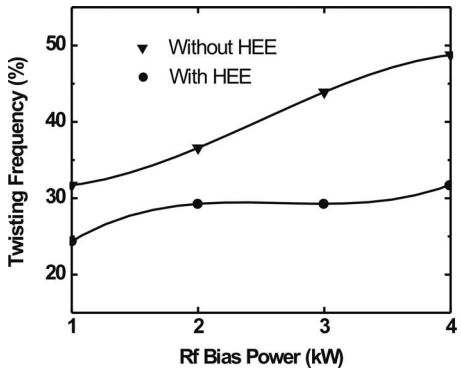

FIG. 12. Twisting probability as a function of rf bias power with and without HEE fluxes for P_{dc}=200 W. The incidence of twisting increases with P_{rf} due to the deeper penetration of ions into the feature before neutralizing. HEE fluxes decrease the incidence of twisting.

twisting frequency with increasing HEE fluxes, the end result is that the twisting frequency increases with increasing rf power.

HAR etching processes are typically performed at high bias powers (many kilowatts) and low frequencies (a few megahertz or less). It is difficult to make specific comments about whether twisting is decreased or enhanced when the bias frequency is lowered or power increased in the absence of detailed studies. Having said that, to first order the incidence of twisting is likely a consequence of statistical variations in the fluxes of radicals, ions and HEE— and in particular their effects on charging. So conditions which minimize these effects will reduce the frequency of twisting. One method to reduce these statistical variations is to increase the magnitude of the fluxes so that the current of particles into the feature is larger. Higher bias powers should increase the magnitudes of fluxes but, as we discussed above, second order effects such as the shape of the IEAD, may offset that benefit. Lower frequencies do not necessarily directly improve upon these statistics by increasing fluxes but do indirectly affect charging by providing IEADs that are generally broader in energy and broader in angle, at least at lower energies. The fact that positive charge may be deposited on the side walls higher in the feature by these lower energy ions is potentially a benefit since the charge is more likely to be neutralized by the thermal electron flux into the feature.

V. CONCLUDING REMARKS

Charging effects on profile evolution have been computationally investigated for HAR SiO_2 features etched in a dc-CCP reactor capable of producing HEE fluxes onto the wafer. Twisting and variations in etch rates were predicted, effects attributed to the stochastic fluxes of reactants into the small features. In the absence of charging, a small incidence of twisting was observed in polymerizing processes due to the random deposition of polymer or random etching on the side walls. Twisting was not observed in nonpolymerizing chemistries for Si (conductor) etching although there was a variation in etch rate due to the stochastic arrival of high energy ions. When including charging but without HEE fluxes, the incidence of twisting increased due to the stochastic production of lateral electric fields inside the feature which deflects ions. The effect is amplified by charge that is trapped in the polymer on the side walls. Highly conductive polymer layers may reduce the frequency of twisting by dissipating charge. In the same manner, thick layers of nonconducting polymer overlying a conductive substrate (e.g., fluorocarbon etching of Si) can produce twisting. When including HEE fluxes, the incidence of twisting was reduced to nearly that in the absence of charging, an affect attributed to the HEE beams neutralizing positive charge deep in the trench. Increasing V_{dc} while the IEADs remain nearly constant increases the HEE flux and the maximum electron energy, both of which reduce the incidence of twisting. Increasing rf bias power generally increases the incidence of twisting by narrowing the angular spread and increasing the energy of the ion flux. Both enable deeper penetration of ions into the feature before undergoing neutralizing collisions. There may also be a contribution to twisting from random statistical variations in material properties, such as composition or structure. These contributions are likely small compared to charging because their range is only as large as the material variation while the effects of charging are felt over large fractions of the feature dimension. UV photon fluxes may also affect twisting through their contribution to surface conductivities.

ACKNOWLEDGMENTS

This work was supported by the Semiconductor Research Corp., Micron Corp., and Tokyo Electron Ltd.

[1] S. Welch, K. Keswick, P. Stout, J. Kim, W. Lee, C. Ying, K. Doan, H. S. Kim, and B. Pu, Semicond. Int. **32**, 18 (2009).
[2] N. Ikegami, A. Yabata, T. Matsui, J. Kanamori, and Y. Horiike, Jpn. J. Appl. Phys., Part 1 **36**, 2470 (1997).
[3] D. Kim and E. A. Hudson, Thin Solid Films **515**, 4874 (2007).
[4] H. S. Park, S. J. Kim, Y. Q. Wu, and J. K. Lee, IEEE Trans. Plasma Sci. **31**, 703 (2003).
[5] A. C. Westerheim, A. H. Labun, J. H. Dubash, J. C. Arnold, H. H. Sawin, and V. Yu-Wang, J. Vac. Sci. Technol. A **13**, 853 (1995).
[6] M. Schaepkens, G. S. Oehrlein, and J. M. Cook, J. Vac. Sci. Technol. B **18**, 856 (2000).
[7] J. Bing, E. A. Edelberg, and T. Yanagawa, U.S. Patent Application No. 2008/0119055 (22 May 2008).
[8] J. C. Arnold and H. H. Sawin, J. Appl. Phys. **70**, 5314 (1991).
[9] S. Samukawa, Appl. Phys. Lett. **64**, 3398 (1994).
[10] G. S. Hwang and K. P. Giapis, Appl. Phys. Lett. **71**, 2928 (1997).
[11] K. P. Giapis, G. S. Huang, and O. Joubert, Microelectron. Eng. **61-62**, 835 (2002).
[12] T. G. Madziwa-Nussinov, D. Arnush, and F. F. Chen, Phys. Plasmas **15**, 013503 (2008).
[13] D. J. Economou, J. Phys. D **41**, 024001 (2008).
[14] A. Ranjan, V. M. Donnelly, and D. J. Economou, J. Vac. Sci. Technol. A **24**, 1839 (2006).
[15] A. Ranjan, C. Helmbrecht, V. M. Donnelly, D. J. Economou, and G. Franz, J. Vac. Sci. Technol. B **25**, 258 (2007).
[16] T. Shimmura, Y. Suzuki, S. Soda, S. Samukawa, M. Koyanagi, and K. Hane, J. Vac. Sci. Technol. A **22**, 433 (2004).
[17] G. S. Sandhu, M. F. Hineman, D. A. Steckert, J. Bai, S. J. Trapp, and T. Schrock, U.S. Patent Application No. 2008/0128389 (5 June 2008).
[18] T. Ohmori, T. Goto, and T. Makabe, J. Phys. D **37**, 2223 (2004).
[19] T. Ohmori and T. Makabe, Appl. Surf. Sci. **254**, 3696 (2008).
[20] M. Wang and M. J. Kushner, J. Appl. Phys. **107**, 023308 (2010).
[21] E. Kawamura, A. J. Lichtenberg, and M. A. Lieberman, Plasma Sources Sci. Technol. **17**, 045002 (2008).
[22] K. Denpoh and P. L. G. Ventzek, J. Vac. Sci. Technol. A **26**, 1415 (2008).
[23] L. Xu, L. Chen, M. Funk, A. Ranjan, M. Hummel, R. Bravenec, R.

Sundararajan, D. J. Economou, and V. M. Donnelly, Appl. Phys. Lett. **93**, 261502 (2008).
[24]M. J. Kushner, J. Phys. D **42**, 194013 (2009).
[25]A. V. Vasenkov, X. Li, G. S. Oehrlein, and M. J. Kushner, J. Vac. Sci. Technol. A **22**, 511 (2004).
[26]A. Sankaran and M. J. Kushner, J. Vac. Sci. Technol. A **22**, 1242 (2004).
[27]C. K. Purvis, "Effects of secondary yield parameter variation on predicted equilibrium potentials of an object in a charging environment," NASA Technical Memorandum 79299, 1979.
[28]V. M. Donnelly, J. Appl. Phys. **79**, 9353 (1996).
[29]J. P. Chang, J. C. Arnold, G. C. H. Zau, H.-S. Shin, and H. H. Sawin, J. Vac. Sci. Technol. A **15**, 1853 (1997).
[30]R. J. Hoekstra, M. J. Grapperhaus, and M. J. Kushner, J. Vac. Sci. Technol. A **15**, 1913 (1997).